Bioresource Technology Reports 17 (2022) 100921

Contents lists available at ScienceDirect

Bioresource Technology Reports

journal homepage: www.sciencedirect.com/journal/bioresource-technology-reports

Removal of minocycline from high concentrated aqueous medium by nonliving and lipid-free *Chlorella* sp. biomass

Karen Saldaña [a], Edgardo Angulo [a], Ivan Mercado [b], Grey Castellar [c], Néstor Cubillán [a,*]

[a] Programa de Química, Facultad de Ciencias Básicas, Universidad del Atlántico, Barranquilla, Colombia
[b] Programa de Ingeniería Agroindustrial, Facultad de Ingenierías, Universidad del Atlántico, Barranquilla, Colombia
[c] Universidad Autónoma del Caribe, Barranquilla, Colombia

ARTICLE INFO

Keywords:
Bioremediation
Minocycline
Microalgae biomass
Adsorption isotherms
Adsorption mechanism

ABSTRACT

This work evaluated the removal of minocycline (MC) by the nonliving Chlorella sp. biomass (NLB) and modified by a lipid extraction procedure (LEB). Both biomasses have different morphology (NLB: globular-like; LEB: flakes and blocks) and size distribution. The pH showed a significant synergistic influence on MC removal ($p < 0.05$). MC initial concentration (C_0) and biomass dosage significantly interact, suggesting that LEB agglomeration decreased removal. NLB removed 90.8 ± 1.3% of MC and LEB 80.8 ± 1.4% at C_0 = 53.89 mg/L, 50 mg of biomass and pH 10. The adsorption kinetics and isotherms suggested multilayer formation by physical and chemical adsorption on heterogeneous and macroporous surfaces. According to results, NLB as an adsorbent had an economic disadvantage because of production costs despite good removal efficiency. However, it is possible to take advantage of the biomass after removing value-added compounds (LEB) as a zero-waste strategy.

1. Introduction

Antibiotics are drugs used for the treatment of diseases affecting human and animal health. These substances increase livestock productivity by using high doses worldwide (Hu et al., 2019). The projection on consumption for agriculture – excluding aquaculture – is 70% in 2030 (Van Boeckel et al., 2015). However, residues in foods, such as milk and meat, exceeded the limit values for human consumption (EnkeMm et al., 2018). Man and animals excreted between 50 and 90% of the consumed drugs through feces and urine and discharged in wastewater treatment plants (Tran et al., 2018).

In low- and medium-income countries, the consumption of antibiotics without prescription is between 19 and 100% (Morgan et al., 2011). The appearance of antibiotic-resistant bacteria in water sources, drinking water, and wastewater treatment plants gained attention worldwide (Sanganyado and Gwenzi, 2019; Tran et al., 2018). There is a projection of ten million deaths in 2050 by these bacteria (Sanganyado and Gwenzi, 2019). In Portugal, in 2011, a study analyzed the resistance of bacteria to MC in soils for agricultural and livestock use, finding 75% of persistence (Sanganyado and Gwenzi, 2019).

MC is a second generation antibiotic derived from tetracycline. It is a broad-spectrum bactericide with high activity and liposolubility. This antibiotic is frequent in livestock feed and aquaculture (Wu et al., 2019). The World Health Organization (WHO) classified this antibiotic in the "Watch" group, antibiotics with a high risk of bacteria resistance and recommended as the first or second choice in treatment options. WHO included these medicines in control and monitoring programs (WHO et al., 2019).

The presence of this antibiotic in effluents is due to households and hospital discharges, and production wastewater. Kümmerer y Lehninger estimated 815 kg/year of MC by hospital and households, from this, 81.5 kg/year are spilled into effluents of Germany in 2003 (Kümmerer and Henninger, 2003). In 2010, Pena et al. reported MC levels of 0.318–0.532 mg/L in four hospital wastewater effluents and 0.350–0.915 mg/L in municipal wastewater treatment plants influents of Coimbra Portugal (Pena et al., 2010). There are no MC data to date for antibiotic production wastewater, but the literature reported between 790 and 899 mg/L of oxytetracycline in industrial wastewater (Liu et al., 2012).

The Minocycline concentration limits are inexistent in most countries' legislation. The European Medicinal Agency defined the environmental risk by comparing the lowest Predicted No Effect Concentration (PNEC) with Predicted Environmental Concentration (PEC). Concentrations below PNEC represent a possible low risk of adverse effects in

* Corresponding author.
E-mail address: nestorcubillan@mail.uniatlantico.edu.co (N. Cubillán).

https://doi.org/10.1016/j.biteb.2021.100921
Received 6 October 2021; Received in revised form 18 November 2021; Accepted 11 December 2021
Available online 16 December 2021

the ecosystem. For Minocycline the Lowest PNEC is 0.21886 mug/L (Aalizadeh et al., 2017). Consequently, there is a need to remove MC from effluents to decrease the risk of spilling into water sources.

The industrial wastewater treatment plants do not have procedures to remove tetracycline-family drugs (Daghrir and Drogui, 2013). Research on removal technology for these drugs becomes necessary. Several techniques have efficiently removed MC from water, such as advanced oxidation processes, coagulation, ion exchange, and adsorption.

The advanced oxidation processes have shown high effectiveness at short contact times; however, the ozonization produces the carcinogenic compound *N*-nitrosodimethylamine (Lv and Li, 2018). Choi et al. found 63–66% MC removal in synthetic and river water, respectively, using coagulation with poly-aluminum chloride. A granular activated carbon removed less than 70% of MC in the same sample (K. J. Choi et al., 2008). Magnetic ion exchange reduced the concentration of MC from 10 to 0.7 μg/L by self-decomposition. The adsorption mechanism removed more than 90% with this material (Choi et al., 2007).

Adsorption is the mechanism commonly involved in MC removal; many techniques require it as the first step. These technologies search for adsorbents with high capacity and selectivity, favorable kinetics, and good mechanical properties. For example, magnetic ordered mesoporous carbon materials (Hu et al., 2019), iron-loaded granular activated carbon catalyst (Pan et al., 2019), and the materials mentioned before have efficiently removed MC in aqueous matrices. However, the costs of these materials can be unreachable in low- and medium-income countries. In this sense, inexpensive technologies, like those based on biomasses represent good options to decrease the MC in industrial wastewater.

Microalgae-based technologies are simple, inexpensive, and efficient to remediate antibiotics. Oxidation ponds use living microorganisms as wastewater treatment methods. Moreover, the nonliving biomass obtained from the microalgae life-cycle is capable of removing contaminants. Additionally, this biomass is a source of lipids for biofuel production with an oil content of 30–70% (Menegazzo and Fonseca, 2019; Sajjadi et al., 2018). In the research group authoring this work, there is an interest in evaluating the suitability of biomass of waste residues from biofuel to remove pollutants. Previously, a report shows ca. 83% of cephalexin removal with nonliving *Chlorella* sp. and the lipid-extracted biomasses (Angulo et al., 2018). This work broadens the biomasses' application spectrum by studying the removal of an antibiotic of tetracycline families, the MC. The results were interpreted based on adsorption mechanisms obtained from kinetics, isotherm experiments, and molecular electrostatic potential of the prototropic species in solution.

2. Methodology

2.1. Nonliving and lipid-extracted Chlorella sp. biomasses preparation

Chlorella (green algae; Chlorophyta) is a freshwater microalga widely distributed in Colombia and worldwide. These microalgae are simple cells with globular shapes, adaptable to closed (bioreactor) and open (ponds) production systems. The biomass production costs are about 2.71 US$/kg (Ye et al., 2018), decreasing 55% with the latest advances in feeding (Hanifzadeh et al., 2018) and harvesting.

The main extracted compounds are lipids for biodiesel production. Moreover, the high value-added compounds (applicable as nutraceuticals, cosmetics, and pharmaceuticals) from residual biomass can generate better economic profit (>100 €/kg for each high value-added compound) (Costa et al., 2020). The carbohydrate- and protein-rich residual biomass have no application. In this sense, a Microalgae Biotechnology Lab. at Universidad del Atlántico (Barranquilla-Colombia) provided the living *Chlorella* sp. strain. It was initially acquired from freshwater and cultured under light stress conditions to increase lipid production.

Table 1
Grid of experiments to evaluate the maximum-removal conditions.

Experiment	pH	m (mg)	C_0 (mg/L)
1	2	40	53.89
2	2	50	47.90
3	2	60	41.92
4	3	40	41.92
5	3	50	47.90
6	3	60	53.89
7	4	40	47.90
8	4	50	53.89
9	4	60	41.92
10	5	40	41.92
11	5	50	53.89
12	5	60	47.90
13	6	40	41.92
14	6	50	53.89
15	6	60	47.90
16	8	40	53.89
17	8	50	47.90
18	8	60	41.92
19	9	40	47.90
20	9	50	41.92
21	9	60	53.89
22	10	40	47.90
23	10	50	53.89
24	10	60	53.89
25	11	40	47.90
26	11	50	53.89
27	11	60	53.89
28	12	40	47.90
29	12	50	41.92
30	12	60	53.89

m: biomass mass; C_0: MC initial concentration.

The procedures of *Chlorella* sp. culture and the preparation of NLB and LEB were detailed in a previous work (Angulo et al., 2018). The culture media consisted of deionized water enriched with the commercial Nutrifoliar fertilizer in a concentration equivalent to 4 mmol/L of nitrogen. The primary inoculum gave 0.100 absorbance units at 647 nm (Shimadzu, UV1800), equivalent to $1 \cdot 10^6$ cells/mL. Cells grown at 27 ± 2 °C for 20 days with constant agitation and aeration. The light/darkness photoperiod was 24 h.

Non-living biomass was obtained after 20 days of suspending the culture. The microalgae were separated by decantation and centrifugation (Hettich, Rotofix 32A). Finally, the *Chlorella* sp. were washed with distilled water and dried in a heating oven (Binder, FD 115-UL) at 70 °C for 12 h, pulverized, and stored for further experiments.

The lipids were extracted from the non-living biomass by a two-step procedure. The first step is the modified Bligh and Dyer (1959), and Guo et al. (2015) protocols: 10 mL of a 2:1 chloroform:methanol (Merck) mixture were added to 50 mg of non-living biomass and sonicated (VWR B1500A-MT, Ultrawave) for 1 h. The obtained mixture was homogenized for 30 s after adding NaCl solution (Panreac, 0.9% w/v). Finally, the mixture was centrifuged (3000 rpm, 8 min) and the organic phase was filtered (1882–047, Whatman). Montes D'Oca et al. described the second step, it is based on a Soxhlet extraction with hexane (Merck, 99.9%) for 5 h (siphon rate of 8–10 cycles/h) (Montes D'Oca et al., 2011). The residual biomass was isolated and washed with 150 mL of a 2:1 mixture of chloroform:methanol. FTIR-ATR (Bruker, Tensor II) and SEM (Quanta, Feg 650) assessed differences between both biomasses.

2.2. Determination of maximum-removal conditions and calibration curve

The maximum-removal conditions were determined by evaluating the apparent MC removal as the response. The evaluation of D-value variation with the number of experiments allowed the selection of the grid size. The Fedorov algorithms produced the grid of experiments by maximizing D-value through the exchange of candidate values of

variables designed. The candidate list of variable values were: (a) pH: 2–6, 8–12, initial MC concentration (C_0(mg/L): 41.92, 47.90, 53.89) and the sorbent mass (m(mg): 40, 50, 60). The idea behind this approach is to propose a set of randomized experiments.

We considered a linear model without interaction. All calculations were carried-out with R and the AlgDesign Library (R Development Core Team, 2016; Wheeler, 2004) Table 1 shows the resulting experimental conditions and the grid of experiments.

For each experiment, 25 mL of MC solution, biomass quantity, and pH were mixed according to the initial concentration, biomass quantity, and pH value given by Table 1. These mixtures were shaken (Digital Orbital Shaker, 200 rpm, 6 h) and centrifuged (Hettich, Rotofix 32) at 3500 rpm for 7 min. The absorption spectrum (Shimadzu, UV1800) between 190 and 450 nm was measured to the supernatant. The apparent removal (%R_{ap}) was calculated using Eq. (1):

$$\%R_{ap} = \frac{A_i - A_f}{A_i} \bullet 100\% \tag{1}$$

where A_i and A_f are the initial and final absorbance of the maximum-absorbance band, respectively. Furthermore, %R_{ap} results were fitted to the linear model:

$$\%R_{ap} = m + C_0 + pH + m^2 + C_0^2 + pH^2 + m\bullet C_0 + m\bullet pH + C_0\bullet pH + m\bullet C_0^2 + m^2\bullet C_0 + m\bullet pH^2 + m^2\bullet pH + pH\bullet C_0^2 + pH^2\bullet C_0 \tag{2}$$

by using ordinary least squares. After an "all subset" variable selection, the influence of variables in terms of the statistical significance were discussed.

For further experiments, the conditions of the experiment whose %R_{ap} value was maximum were selected. Under these conditions, the calibration curves were prepared without biomass (treatment 0) and with biomass (non-living biomass: treatment 1; lipid-extracted biomass: treatment 2) taking a contact time close to zero. ANCOVA analysis was performed to determine the effect of the biosorbent on the calibration curve.

2.3. Removal profiles and adsorption kinetics

A solution with 25 mL of MC solution (C_0), biomass quantity (m_b), and pH was prepared with the initial concentration, biomass mass, and pH value where %Rap was a maximum. The absorbance spectrum was recorded at 1, 15, 30, 60, 120, 180, 240, 300, 360 min. The adsorption capacity at time t (q_t) and the removal efficiency (% R) were calculated from Eqs. (2) and (3), respectively (Tran et al., 2017).

$$q_t = (C_0 - C_t)\frac{V}{m_b} \tag{3}$$

$$\%R = \left(\frac{C_0 - C_t}{C_0}\right) \bullet 100\% \tag{4}$$

where C_0 and C_t are the concentrations (mg/L) at times zero and t. This concentration was calculated from the calibration curve at maximum-removal conditions. V is the solution volume (0.025 L) of the MC solution and y m_b the biomass mass (mg).

The q_t and time(t) data were fitted to the Pseudo-First-Order [Eq. (5)], Pseudo-Second-Order [Eq. (6)], Elovich [Eq. (7)] and intraparticle diffusion [Eq. (8)] (Tran et al., 2017):

$$q_t = q_e\left(1 - e^{-k_1 t}\right) \tag{5}$$

$$q_t = \frac{q_e^2 k_2 t}{1 + q_e k_2 t} \tag{6}$$

$$q_t = \frac{1}{\beta} ln(1 + \alpha\beta t) \tag{7}$$

$$q_t = k_p t^{1/2} + C \tag{8}$$

where q_e (mg·g^{-1}) is the equilibrium adsorption capacity, k_1 (min^{-1}) and k_2 (g·mg^{-1}·min^{-1}) are the rate constants of pseudo-first-order and pseudo-second-order, respectively; α (mg·g^{-1}·min^{-1}) is the initial rate constant and β (g·mg^{-1}) is the desorption constant in the Elovich model. K_p is the rate constant and C is a constant proportional to the extent of the boundary layer thickness, respectively (McKay et al., 1980). All of isotherms parameters were determined by two fitting procedures: Linear and Nonlinear. In the linear procedure, the ordinary least squares on the linearized equations allowed the data fitting. The nonlinear fitting procedure was performed on the original equations with the Gauss-Newton algorithm. All calculations were carried out with R (R Development Core Team, 2016).

2.4. Adsorption equilibrium

The adsorption capacity, q_e, was determined by mixing 25 mL of MC solution with the biomass at 25 °C. The experiments were conducted at the maximum-removal conditions. The containers were shaken at 150 rpm for the equilibrium time given by the adsorption kinetics results. Absorbance at 298 nm was recorded before and after stirring, and the MC concentrations were determined with the calibration curve. These results were fitted to the Freundlich [Eq. (9)](Tran et al., 2017), Brunauer-Emmet-Teller [BET, Eq. (10)](Ebadi et al., 2009) and Frenkel-Halsey-Hill [FHH, Eq. (11)](Saadi et al., 2015) isotherms:

$$q_e = K_f C_e^{1/n} \tag{9}$$

$$q_e = \frac{q_{max} C_{BET} C_e / C_s}{(1 - C_e/C_s)(1 - C_e/C_s + C_{BET} C_e/C_s)} \tag{10}$$

$$q_e = q_m d\left(\frac{RT}{\alpha} ln\left(\frac{C_e}{C_s}\right)\right)^{-1/r} \tag{11}$$

where K_f is the Freundlich equilibrium constant, C_e is the equilibrium concentration (mg/L), and 1/n is related to the adsorbate-adsorbent affinity. In Eq. (9), q_{max} is maximum adsorption capacity, C_{BET} is the BET constant and C_s is the saturation concentration. In Eq. (11), d is the distance between layers (m), α is the isothermal constant (J m^r mol^{-1}), and r is the distance from the surface to the last layer, respectively.

In the Freundlich model, the ordinary least squares for the linearized equation and the Gauss-Newton for the nonlinear equation were used to fit the data. For the BET and FHH models, the fit procedure was performed with genetic algorithms (GA) (population = 1000, generations = 1000, crossover rate = 50%, mutation rate = 10%) followed by an optimization with the Broyden-Fletcher-Goldfarb-Shanno algorithm (BFGS) (Scrucca, 2013).

2.5. Density functional theory calculations

The description of prototropic species of minocycline were performed by the molecular electrostatic potential calculated from the

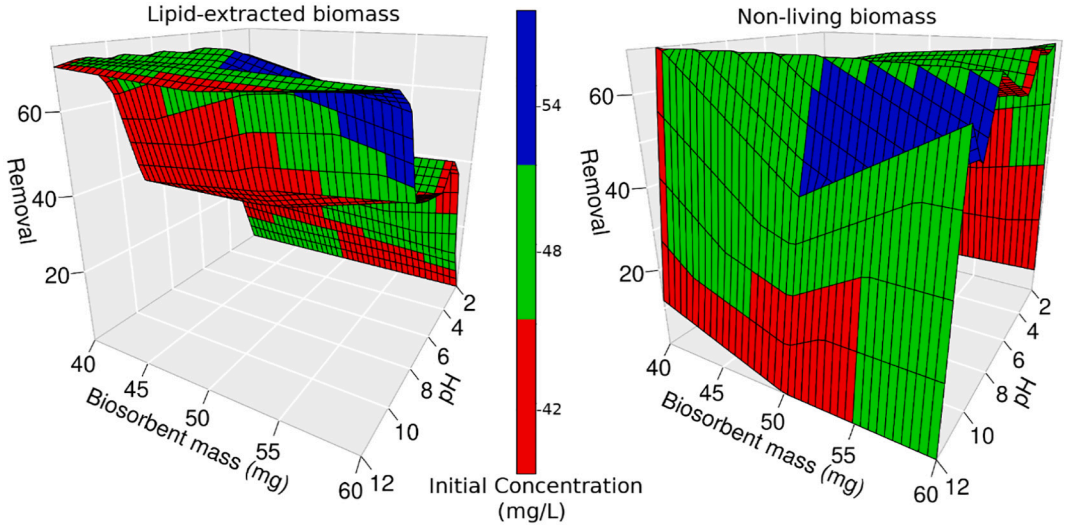

Fig. 1. Response surface for MC apparent removal with lipid-extracted (left) and nonliving (right) Chlorella sp., biomasses.

Table 2
Linear regression models for response surface of R_{ap} as function of initial concentration (C_0), biosorbent dosage (m), and pH.

Parameter	Estimate ± std. error	*t*-value	$p(>\|t\|)$
Lipid-free biomass (LEB)			
Intercept	$(3.212 \pm 0.962) \times 10^3$	3.340	0.00285
C_0	-65.95 ± 19.59	−3.367	0.00267
m	-129.8 ± 39.23	−3.308	0.00307
pH	6.258 ± 0.542	11.530	4.88×10^{-11}
m^2	1.274 ± 0.391	3.261	0.00344
$C_0 : m$	2.656 ± 0.796	3.336	0.00287
$C_0 : m^2$	$-(2.602 \pm 0.792) \times 10^{-2}$	−3.287	0.00323
Non-living biomass (NLB)			
Intercept	$-(4.944 \pm 2.482) \times 10^3$	−1.992	0.0589
C_0	$(2.118 \pm 1.047) \times 10^2$	2.023	0.0554
m	95.57 ± 50.60	1.889	0.0722
pH	32.25 ± 4.412	7.309	2.56×10^{-7}
C_0^2	-2.258 ± 1.095	−2.062	0.0512
pH^2	-2.394 ± 0.316	−7.582	1.42×10^{-7}
$C_0 : m$	-4.133 ± 2.136	−1.935	0.0660
$C_0^2 : m$	$(4.416 \pm 2.233) \times 10^{-2}$	1.978	0.0606

optimized structures. The electronic structure calculations was realized in the Density Functional Theory (DFT) with the M06-2× functional and the basis set 6–311 + g(d,p). A vibrational analysis on the optimized structures confirmed the absence of negative eigenvalues in the Hessian matrix. All calculations were performed with Gaussian 09 Rev. A02 (Frisch et al., 2009).

3. Results and discussion

3.1. Biomass characterization

FTIR spectrum of LEB and NLB showed the typical absorption bands of proteins, amide I, II, and III at ~1650, ~1550, and 1400–1200 cm^{-1}, respectively. There are no observed differences between the band's intensities for both biomasses, i.e., the proteins content was not modified. After the lipid extraction procedure, the band's intensities at 900–1000, 1100, 1250, and 1050 cm^{-1} decreased, indicating a decrease of the carotenoids, nucleic acids, phospholipids, and carbohydrates content. The fatty acids and lipids bands (1730–1750 cm^{-1}) disappeared, confirming the extraction of lipids in the matrix.

SEM results revealed differences in particles shape and size distribution between both biomasses. NLB has a globular-like shape with a size between 20 and 50 μm (see E-supplement). LEB formed flakes, blocks, and elongated particles, suggesting agglomerative processes. In this biomass, the particle size ranged from 2 to 400 μm.

3.2. Maximum-removal conditions and calibration curves

Fig. 1 shows the response surface for apparent MC removal (%R_{ap}) with NLB and LEB. LEB showed an ascending step behavior with the increasing pH. For NLB, the surface has an inverted U shape. The apparent removal has a maximum at pH 10, $C_0 = 53.89$ mg/L, and $m_b =$ 50 mg of biomass; these conditions were kept for both treatment, nonliving microalgae, and post-lipid extraction microalgae.

The linear models obtained from least-squares fitting and variable selection are shown in Table 2. The determination coefficient (R^2) was 0.87 for LEB and 0.73 for NLB. The ANOVA test for the model revealed that the LEB model was significant (p(LEB) $= 5.36 \times 10^{-9}$) while NLB showed a p(LEB) $= 1.3 \times 10^{-4}$.

The pH has a significant effect ($p < 0.05$), %R_{ap} increased with the increasing pH, in both biomasses. Fig. 2A and B exhibit the linear dependence of apparent removal with pH, while the downward parabola is evidence of quadratic term with a negative coefficient of NLB (Fig. 2, b1 and b2). Despite the strong influence of pH, it has no interactions with other variables (Fig. 2C, and Table 2).

In the literature, there are various reports on the effect of pH on MC removal. Using CeO_2 as an adsorbent, the adsorption is relatively high at pH 4.4 and significantly decreases at pH 7 and 9.5, indicating a high affinity of MC for the CeO_2 surface at low pH (Brigante and Schulz, 2012a). Similar results were found for MC removal by montmorillonite since the surface of this clay is negative (Parolo et al., 2010).

In other reports, the change in pH had a non-significant effect on the MC adsorption on the porous 3D structures of γ-AlO(OH)/MgAl-LDH/C (J. Li et al., 2015) and magnetic microspheres of $MgFe_2O_4$/γ-Fe_2O_3 (Lu et al., 2016). It was concluded that this behavior is a consequence of the diversity of the charged nature of sites and the amphoteric properties of MC at different pH (Lu et al., 2016).

The MC initial concentration (C_0) and the biomass dosage (m) showed a significant effect for the removal in LEB (see Table 2). The C_0 has an antagonist effect on $\%R_{ap}$, i.e., the removal decreases with the increasing MC initial concentration. The biomass dosage exhibits an upward parabola behavior (See Table 2). Additionally, the significance and the coefficient signs of $C_0 : m$ and $C_0 : m^2$ suggest a synergistic effect between these variables. At pH 10, this interaction induces a change on C_0 effect at the maximum m (see Fig. 2E).

Multilayer formation by MC and agglomerative processes of LEB possibly justified the observed removal behavior. At low MC

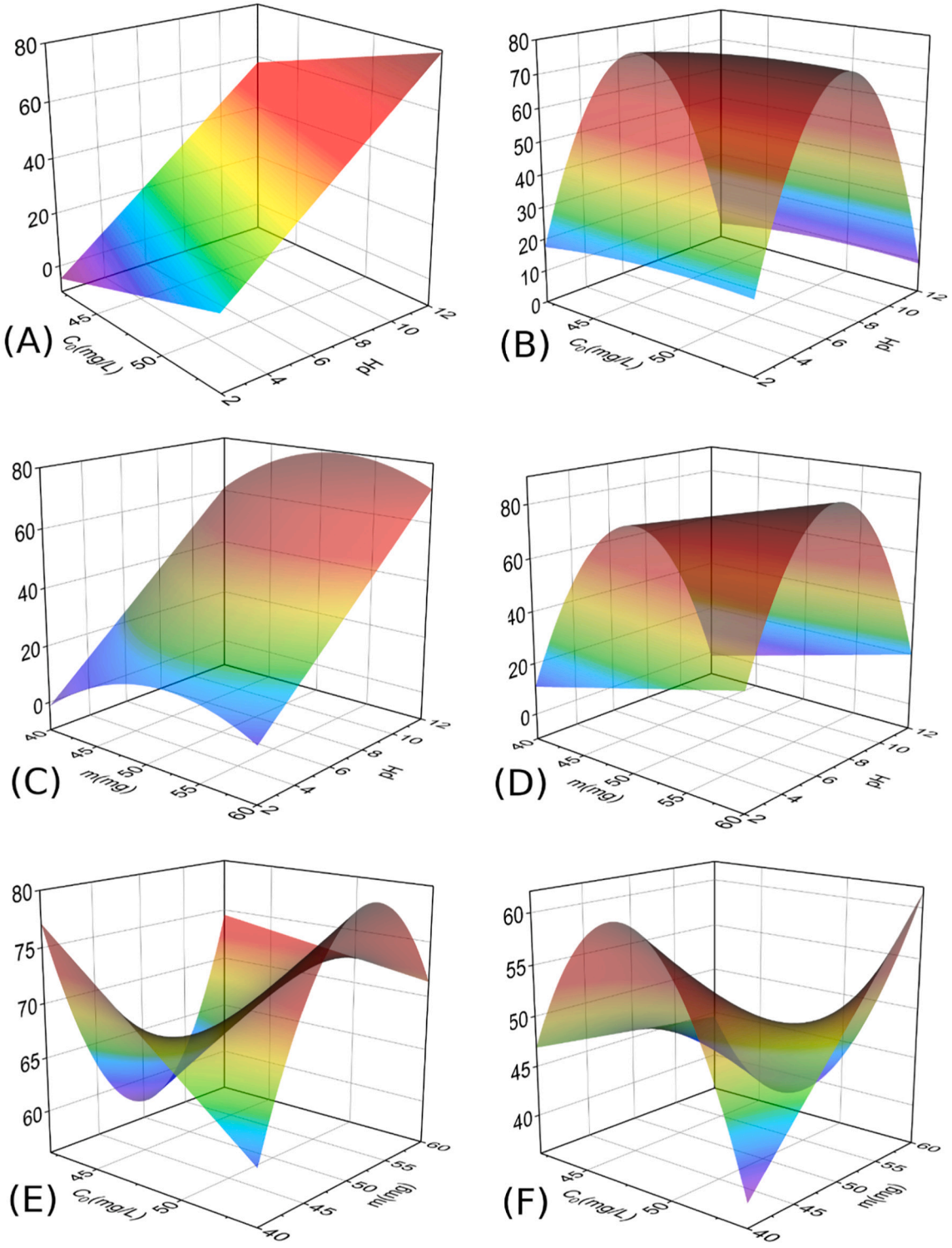

Fig. 2. Surface response plots of apparent removal of MC with LEB (A, C, E) and NLB (B, D, F). A and B are the C_0 vs. pH biplot at 50 mg of biomasses. C and D are the *m* vs. pH biplot at 53.89 mg/L of initial MC concentration. E and F are the C_0 vs. *m* biplot at pH 10. The *z*-axis is the MC apparent removal.

concentration and low adsorbent dosage there are high availability of active sites. On the increasing biomass dosage and initial MC concentration, the agglomerative and adsorptive processes compete lowering active sites, and promoting multilayer formation. If the MC initial concentration increases, desorption takes place.

For NLB, the $p(>|t|)$ were slightly greater than 0.05 for these variables and interactions; therefore, the interpretation is not reliable at this significance level. However, a comparison with LEB is plausible. The trends of $\%R_{ap}$ with C_0 and m are inverted by NLB. There is an increasing $\%R_{ap}$ with the increasing C_0, and the biomass dosage exhibits a downward parabola (See Table 2).

At pH 10, the increasing biomass dosage at low MC concentration holds $\%R_{ap}$ nearly constant. With 50 mg/L of MC, the descending trend of $\%R_{ap}$ indicates a probable agglomerative process of biomass competing with adsorption. This tendency is reverted at 60 mg/L of MC, suggesting a high contribution from desorption at low m, and the

Table 3
MC removal profiles using non-living (NLB) and lipid-extracted (LEB) Chlorella sp., biomasses.

t(min)	%R(NLB)	%R(LEB)
0	0.00 ± 2.9	0.00 ± 2.9
15	67.7 ± 1.6	69.2 ± 1.5
30	79.1 ± 1.4	72.1 ± 1.5
60	85.0 ± 1.4	75.2 ± 1.5
120	86.0 ± 1.4	71.2 ± 1.5
180	87.3 ± 1.4	72.2 ± 1.5
240	87.3 ± 1.4	75.2 ± 1.4
300	88.1 ± 1.4	80.5 ± 1.4
360	90.8 ± 1.3	80.8 ± 1.4

increment of active sites and multilayer formation at high *m* (see Fig. 2F).

The UV-VIS spectrum and the calibration curves data of MC solution are shown in the *E*-supplement. At pH 10, MC in aqueous solution has three UV-VIS absorption maxima at 244.4 nm (λ_1), 272.8 nm (λ_2), and 383.6 nm (λ_3). The ANCOVA revealed no significant interaction ($p > 0.05$) between concentration and biomass (treatment 0: without biomass, treatment 1: NLB, and treatment 2: LEB) for λ_1 and λ_3. Moreover, there are non-significant differences between the slopes of the three calibration curves. At 383.6 nm (λ_2) the determination coefficient was 0.999, selecting this as working wavelength. Conversely, significant differences ($p < 0.05$) exist between the slopes at λ_2.

3.3. Removal efficiency and adsorption kinetics

Table 3 shows the results of the MC removal profile in aqueous solutions using NLB and LEB. The equilibrium reached at 180 and 300 min, respectively, and it is consistent with the observed trend in the response surface (Fig. 2). NLB surface is quickly saturated, and desorption can occur after the maximum-removal initial concentration. Conversely, LEB tends to agglomerate before the surface saturation.

The literature reported equilibrium times greater than those obtained in this work. Porous magnetic microspheres of γ-Fe_2O_3 and $MgFe_2O_4$/γ-Fe_2O_3 reached equilibrium in 48 h for both materials (Lu et al., 2016). In another study, the equilibrium of removal occurred at ten h with 3D hierarchical structures of CLDH/γ-AlO(OH)-2-500, LDH/γ-AlO(OH)/C-2, and LDH-2 (J. Li et al., 2015a). Conversely, in adsorption experiments performed with mesoporous carbon materials doped with Fe_3O_4 magnetic particles, Fe_3O_4-OMC-1.5 reached the equilibrium in 10 min (Hu et al., 2019).

A comparison of the efficiency in MC removal showed that NLB removed 90.8 ± 1.3% while LEB is 80.8 ± 1.4%. This difference occurs by the change in the properties of the cell wall; the lipid extraction eliminates available binding sites. However, LEB achieved a good removal giving a potential use to a by-product of lipid extraction. It can be identified as a viable zero residue strategy to improve the sustainability of microalgae cultivation (Guo et al., 2016).

Our results showed a better performance than coagulation with polyaluminum chloride, 63 and 66%, and adsorption with a granular activated carbon (70%) (K. J. Choi et al., 2008a). The magnetic ion-exchange showed a removal efficiency of 93%, of which 90% is by adsorption mechanism (Choi et al., 2007). Moreover, the adsorption-based methods were slightly more efficient, e.g., coal activated carbon removed MC more than 90% (K. Choi et al., 2008a).

The data of q_t followed a pseudo-second-order kinetics (see Fig. 3) with $R^2 = 0.999$ for NLB and $R^2 = 0.994$ for LEB (Table 4). Adsorption studies of MC with CLDH/γ-AlO(OH)-2–500, LDH/γ-AlO(OH)/C-2, LDH-2 (J. Li et al., 2015a), γ-Fe_2O_3, and $MgFe_2O_4$/γ- Fe_2O_3 supported the observed behavior (Lu et al., 2016). On the other hand, the ordinary least squares fit on the linearized equation given the best results than the nonlinear fit.

The adsorption capacity in equilibrium (q_e) and the rate constant of the pseudo-second-order model (k_2) were greater in NLB [24.3(2) $mg{\cdot}g^{-1}$ and 9.83 (4.38) × 10^{-3} g mg^{-1} min^{-1}, respectively] than LEB [21.5(4) $mg{\cdot}g^{-1}$ and 9.26(7.15) × 10^{-3} $g{\cdot}mg^{-1}{\cdot}min^{-1}$ in that order],

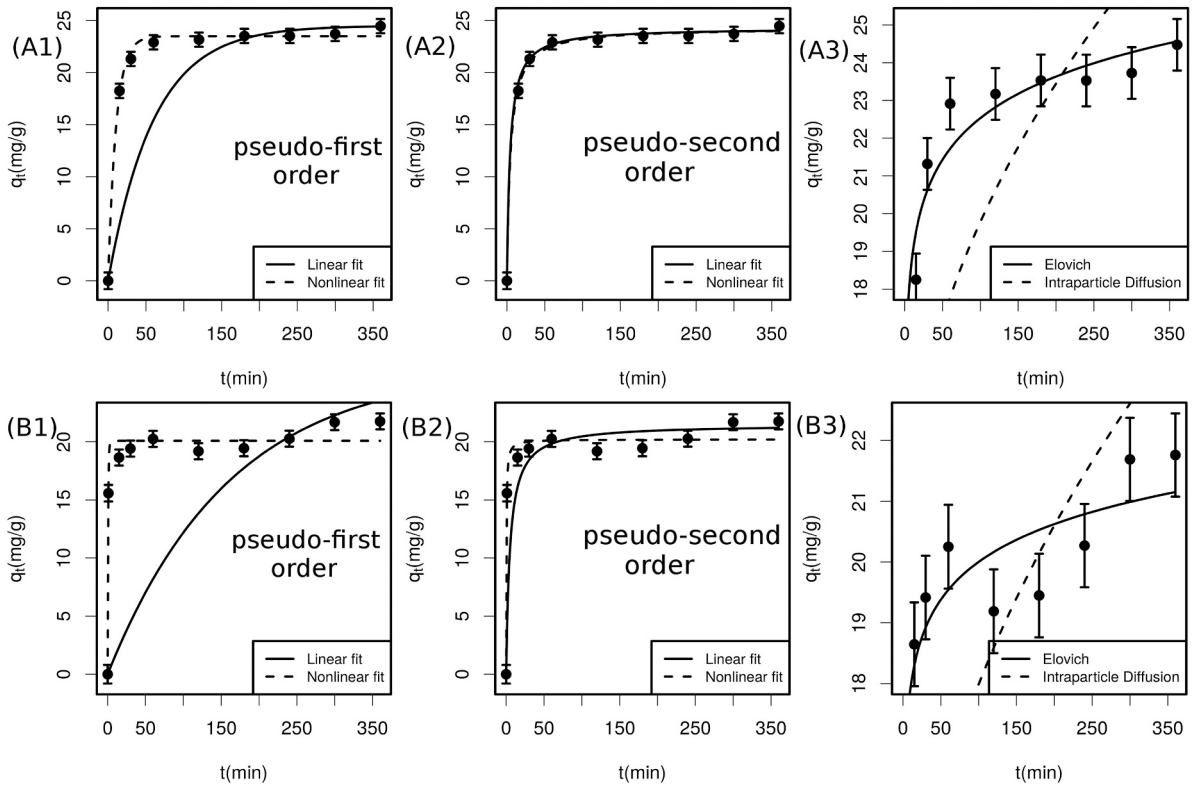

Fig. 3. MC adsorption kinetics results using (A) non-living and (B) lipid-extracted *Chlorella* sp., biomasses.

Table 4
MC adsorption kinetics results using (A) non-living and (B) lipid-extracted Chorella sp., biomasses fitted to different models.

	Pseudo-first order			
Sorbent/fit method	q_e(mg·g^{-1})	k_1(min^{-1})	R^2	Ref.
NLB/NL	23.5(2)	0.0948 (65)	0.995	TW
LEB/NL	20.1(4)	1.50(25)	0.975	TW
CLDH/γ-AlO(OH)-2-500	288.6	4.92	0.9018	(L. Li et al., 2015)
LDH/γ-AlO(OH)/C-2	302.5	3.9	0.9467	(L. Li et al., 2015)
LDH-2	200.5	4.02	0.9475	(L. Li et al., 2015)
γ-Fe_2O_3	83.52	26.958	0.8857	(Lu et al., 2016)
$MgFe_2O_4$/γ-Fe_2O_3	61.43	42.156	0.9917	(Lu et al., 2016)

	Pseudo-second order			
	q_e(mg·g^{-1})	k_2(g·mg^{-1}·min^{-1})	R^2	
NLB/L	24.3(2)	9.83(4.38) × 10^{-3}	0.999	TW
NLB/NL	24.3(2)	8.73(71) × 10^{-3}	0.998	TW
LEB/L	21.5(5)	9.26(7.15) × 10^{-3}	0.994	TW
LEB/NL	20.2(4)	0.159(47)	0.979	TW
CLDH/γ-AlO(OH)-2-500	307.4	0.03768	0.9956	(L. Li et al., 2015)
LDH/γ-AlO(OH)/C-2	334.9	0.03522	0.9943	(L. Li et al., 2015)
LDH-2	224	0.1068	0.9965	(L. Li et al., 2015)
γ-Fe_2O_3	83.82	0.5274	0.9956	(Lu et al., 2016)
$MgFe_2O_4$/γ-Fe_2O_3	63.82	0.5244	0.9991	(Lu et al., 2016)

	Elovich			
	β(mg·g^{-1})	α(mg·g^{-1}·min^{-1})	R^2	
NLB	0.630(107)	2.32(13.5) × 10^4	0.850	TW
LEB	1.11(18)	4.30(26.65) × 10^7	0.846	TW

	Intra-particle diffusion			
	C	k_p(mg·g^{-1}·min$^{1/2}$)	R^2	
NLB	10.9(3.6)	0.885(302)	0.550	TW
LEB	11.7(2.8)	0.631(248)	0.446	TW

NLB: non-living biomass; LEB: lipid-extracted biomass; L: Linear fit; NL: Nonlinear fit; TW: this work.

supporting that observed before from the removal results.

The Elovich model was not adequate to describe the experimental data of the adsorption of MC in NLB ($R^2 = 0.850$) and LEB ($R^2 = 0.846$). This model assumes that the surface of NLB and LEB is energetically heterogeneous (Zhou et al., 2017).

Table 5
MC adsorption isotherms results using non-living and lipid-extracted Chorella sp., biomasses.

		Freundlich			
Sorbent	pH	K_F(mg·g^{-1})	1/n	R^2	Ref.
NLB/L	10	1.17(42)	1.44 (19)	0.923	TW
LEB/L	10	0.138(52)	1.95 (16)	0.957	TW
CeO_2	4.4	0.113	0.118	0.989	(Brigante and Schulz, 2012b)
	7.0	0.264	0.278	0.99	
	9.5	0.113	0.118	0.989	
Fe-SiO_2	4.4	32.86	0.338	0.995	(Brigante et al., 2014)
	7.0	4.2	0.613	0.999	
	9.5	0.52	0.870	1	
SiO_2	4.4	1.38	0.758	0.999	(Brigante et al., 2014)
	7.0	0.38	0.909	0.999	
	9.5	0.27	0.926	0.999	
Fe_3O_4-OMC-1.5	–	82.37	0.408	0.9699	(Hu et al., 2019)

	Frenkel-Halsey-Hill					
	q_s(mg·g^{-1})/d	R	C_s(mg/L)	α (J/mol)	R^2	
NLB/GA + BFGS	8.06	2.69	8.83	5476	0.961	TW
LEB/GA + BFGS	4.36	0.574	27.3	4503	0.944	TW

	BET				
	q_{max}(mg·g^{-1})	C_{BET}(L·mg^{-1})	C_s(mg/L)	R^2	
NLB/GA + BFGS	57.8	0.653	22.5	0.990	TW
LEB/GA + BFGS	85.0	0.226	31.0	0.987	TW

NLB: Non-living biomass; LEB: Lipid-extracted biomass; L: Linear fit; NL: Nonlinear fit; GA + BFGS: Genetic Algorithms followed by optimization with Broyden–Fletcher–Goldfarb–Shanno Algorithm; TW: this work.

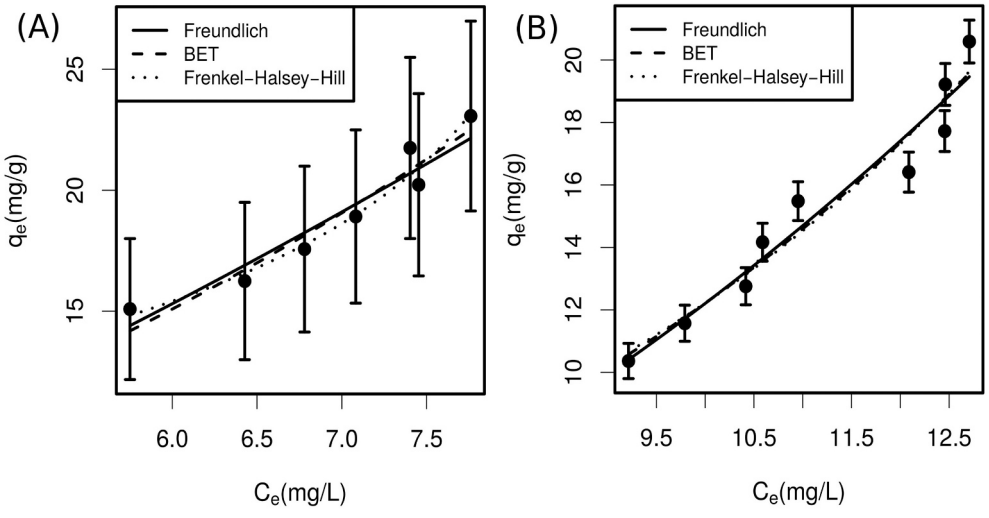

Fig. 4. MC adsorption isotherms using (A) non-living and (B) lipid-extracted Chlorella sp., biomasses.

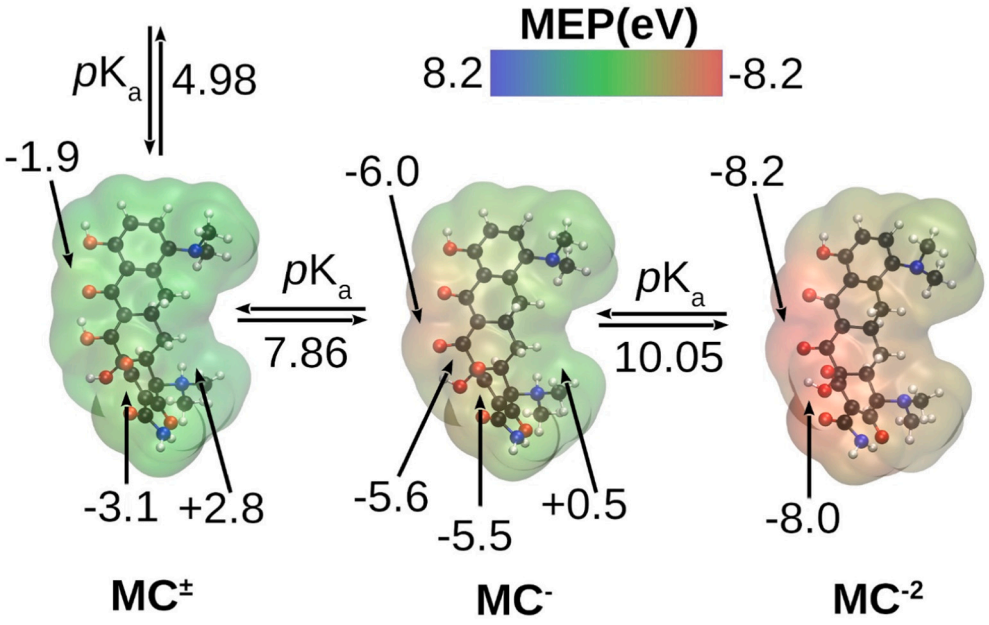

Fig. 5. Molecular electrostatic potential of prototropic species of minocycline (MC). Arrows signal the maxima and minima molecular electrostatic potential.

3.4. Adsorption equilibrium

Fig. 4 shows the adsorption isotherms for MC in both biomasses. The convex shape resembles the type III isotherm according to the IUPAC classification, and it suggests a typical behavior for multilayer adsorption with weak adsorbate-adsorbent interactions and relatively strong adsorbate-adsorbate interactions. Also, there is no restriction in the adsorption process, and the adsorbent has macropores (Bushra et al., 2017).

Table 5 summarizes the obtained parameters from fitting the data to the Freundlich, BET, and FHH isotherm models, and Fig. 4 shows the fitted curves. Adsorption capacity data using NLB and LEB fitted to the Freundlich model (R^2 = 0.923–0.957) suggested adsorption on a heterogeneous surface. The observed results of the parameter of the Freundlich constant (K_F) indicate more favorable adsorption by NLB [1.17(42) mg g^{-1}] than LEB [0.138 (52) mg g^{-1}], supporting the results of kinetics results.

The value of 1/n, 1.44 for NLB, and 1.95 for LEB reveals an unfavorable adsorption process, as usual for a type III isotherm. These results suggest that physisorption (electrostatic, weak hydrogen bonds, and van der Waals) drives the removal process (Zhang et al., 2015).

A comparison with literature showed several adsorbents fitting to the Freundlich isotherm (R^2 ~ 1.0), such as CeO_2 (Brigante and Schulz, 2012a), Fe-SiO_2, SiO_2 (Brigante et al., 2014), and Fe_3O_4-OMC-1,5 (Hu et al., 2019). However, 1/n and K_F values suggested a better affinity of these adsorbents towards MC adsorption (See Table 5).

The FHH isotherm also achieved a good fit of the adsorption data for NLB and LEB with R^2 of 0.961 and 0.944, respectively. This model describes multilayer adsorption, assuming a variation of adsorption potential based on distance from the adsorbed molecule to the adsorbent surface, assumes that surface heterogeneity affects adsorption on all adsorbed layers (Saadi et al., 2015).

The value of α is related to the long-range van der Waals interactions between the surface and the first layer of adsorbed molecule and interactions between neighboring adsorbate molecules containing information about the adsorption capacity of the surface (Alver and Metin, 2012). For NLB and LEB, it was 5476 and 4503 J•mol^{-1}, and the adsorbate monolayer saturation concentration (q_s/d) values for both biosorbents are NLB 8.06 mg·g^{-1}·m^{-1} and LEB 4.36 mg·g^{-1}·m^{-1}, respectively. It was consistent with that observed for the affinity of MC by the biomasses.

The maximum adsorption capacity (q_{max}) was greater for LEB (85.0 mg·g^{-1}) than NLB (57.8 mg·g^{-1}) and, similarly, the saturation concentration (C_s) for BEL (31.0 mg/L) and NLB (22.5 mg/L). This result indicates a contradiction with the information given by the Freundlich isotherm. However, the C_{BET} constant revealed that the first layer formation is more favored than the formation of subsequent layers in NLB (0.653 L·mg^{-1}). Conversely, in LEB (0.226 L·mg^{-1}), the formation of the subsequent layers is more favored. It is noteworthy, the C_{BET} parameter is the relationship between the equilibrium constants of the first layer and subsequent layers formation (Ebadi et al., 2009).

3.5. DFT calculations and adsorption mechanism

In pH values greater than 9, MC species coexist as an equilibrium between the monoanionic (MC^-) and dianionic species (MC^{-2}), see Fig. 5. In this work, the greater MC removal was obtained at pH greater than 10 in NLB and LEB. Consequently, the before mentioned species (MC^- and MC^{-2}) are the most abundant.

The molecular electrostatic potential shows the negative charge concentration in the oxygen zone, hydroxyl and ketone groups in keto-enol tautomerism. The positive charge is located around the amino and ammonium fragments. As the prototropic species change from zwitterion to MC^- and MC^{-2}, the negative electrostatic potential increases (1.9–3 ➔ ~ 5 ➔ ~ 8 eV), and the positive electrostatic potential decreases (see Fig. 5).

Analyzing the structure of MC complexes with proteins, it is possible to infer the importance of charged centers of MC in complexation. Palm et al. reported the crystal structure of the TETR(D) E147A mutant in complex with MC and magnesium (Palm et al., 2020). The negative region of MC was capable of interacting with cations, such as protons and metals. The positive regions showed contacts through hydrogen bonds with amino acid carbonyls and NH···π interactions with phenylalanine.

Also, the formation of complexes with several MC units has been reported. As an example, MC occupies the hydrophobic pockets of the Secretory Phospholipase A_2, forming an MC trimer. Water molecules bridge the units through hydrogen bonds. Additionally, T-shaped OH···π interactions were observed (Dalm et al., 2010). This report supports the formation of clusters or multilayer of MC observed in this work.

The multiple functional groups in the biomasses provide a heterogeneous surface with different sites capable of adsorbing MC with different energies. In the whole pH range (2−12), the biomass active adsorption sites, functional groups such as RCOOH, R_2CO, RNH_2, RSH, and ROH favored the ion exchange promoting electrostatic interactions, hydrogen bonds, and van der Waals interactions. In the case of lipid extracted biomass, the number of functional groups on the surface decreased by the extraction process. These include plastid and glycolipids (monogalactosyldiacylglycerol, digalactosyldiacylglycerol, and sulfoquinovosyldiacylglycerol), phosphoglycerolipids (phosphatidylglycerol, phosphatidylcholine, phosphatidylethanolamine, phosphatidylserine, and phosphatidylinositol), sphingolipids, and neutral lipids such as diacylglycerol (Martin et al., 2014). The lipophilic MC found fewer lipophilic sites to adsorb and fewer lipid negative heads to promote ion-exchange.

Both biomasses are suitable for chemical changes to improve the removal capacity. The high pH values for removal suggest that basic treatments create negative sites on the surface, and the positive region of MC interacts with the formed sites. On the other hand, posterior doping with metal ions, as Mg^{+2} or Fe^{+2}, possibly neutralizes the one negative surface charge creating one positive charge. This modification allows the negative side of MC to interact with the new surface.

4. Conclusions

This work evaluated the removal of minocycline by non-living *Chlorella* sp. (NLB) and lipid-extracted biomasses (LEB). LEB removed 80.8% of minocycline and NLB 90.8%. The morphology, size distribution, and biomolecules content of both biomasses are different. High pH values favored minocycline removal; initial concentration and biomass dosage influence depended on the biomass. The adsorption kinetics and isotherms suggested multilayer formation by physical and chemical adsorption on heterogeneous and macroporous surfaces. NLB is not an economically favored adsorbent because of production costs despite their removal efficiency. However, LEB is a promising material based on a zero-waste strategy.

CRediT authorship contribution statement

Karen Saldaña: Methodology, Investigation, Validation. **Edgardo Angulo:** Writing – review & editing, Project administration, Funding acquisition. **Ivan Mercado:** Resources, Writing – review & editing. **Grey Castellar:** Methodology, Data curation. **Néstor Cubillán:** Conceptualization, Formal analysis, Writing – original draft.

Declaration of competing interest

The authors declare that they have no known competing financial interests or personal relationships that could have appeared to influence the work reported in this paper.

Acknowledgements

The authors thank Ministerio de Ciencias, Tecnología e Innovación de Colombia (Project: “Remoción de antibióticos mediante la biomasa residual de microalgas después de extracción de lípidos”, grant number: 64514) for financial support.

References

Aalizadeh, R., von der Ohe, P.C., Thomaidis, N.S., 2017. Prediction of acute toxicity of emerging contaminants on the water flea Daphnia magna by ant colony optimization-support vector machine QSTR models. Environ Sci Process Impacts 19, 438–448. https://doi.org/10.1039/C6EM00679E.

Alver, E., Metin, A.Ü., 2012. Anionic dye removal from aqueous solutions using modified zeolite: adsorption kinetics and isotherm studies. Chem. Eng. J. 200–202, 59–67. https://doi.org/10.1016/j.cej.2012.06.038.

Angulo, E., Bula, L., Mercado, I., Montaño, A., Cubillán, N., 2018. Bioremediation of Cephalexin with non-living Chlorella sp., biomass after lipid extraction. Bioresour. Technol. 257, 17–22. https://doi.org/10.1016/j.biortech.2018.02.079.

Bligh, E.G., Dyer, W.J., 1959. A rapid method of total lipid extraction and purification. Can. J. Biochem. Physiol. 37, 911–917. https://doi.org/10.1139/o59-099.

Brigante, M., Schulz, P.C., 2012a. Adsorption of the antibiotic minocycline on cerium (IV) oxide: effect of pH, ionic strength and temperature. Microporous Mesoporous Mater. 156, 138–144.

Brigante, M., Schulz, P.C., 2012b. Cerium (IV) oxide: synthesis in alkaline and acidic media, characterization and adsorption properties. Chem. Eng. J. 191, 563–570.

Brigante, M., Parolo, M.E., Schulz, P.C., Avena, M., 2014. Synthesis, characterization of mesoporous silica powders and application to antibiotic remotion from aqueous solution. Effect of supported Fe-oxide on the SiO2 adsorption properties. Powder Technol. 253, 178–186.

Bushra, R., Ahmed, A., Shahadat, M., 2017. Mechanism of adsorption on nanomaterials. In: RSC Detection Science. Royal Society of Chemistry, pp. 90–111. https://doi.org/10.1039/9781782623625-00090.

Choi, K.-J., Son, H.-J., Kim, S.-H., 2007. Ionic treatment for removal of sulfonamide and tetracycline classes of antibiotic. Sci. Total Environ. 387, 247–256. https://doi.org/10.1016/j.scitotenv.2007.07.024.

Choi, K.J., Kim, S.G., Kim, S.H., 2008. Removal of antibiotics by coagulation and granular activated carbon filtration. J. Hazard. Mater. 151, 38–43. https://doi.org/10.1016/j.jhazmat.2007.05.059.

Costa, J.A.V., Freitas, B.C.B., Moraes, L., Zaparoli, M., Morais, M.G., 2020. Progress in the physicochemical treatment of microalgae biomass for value-added product recovery. Bioresour. Technol. 301, 122727 https://doi.org/10.1016/J.BIORTECH.2019.122727.

Daghrir, R., Drogui, P., 2013. Tetracycline antibiotics in the environment: a review. Environ. Chem. Lett. 11, 209–227. https://doi.org/10.1007/s10311-013-0404-8.

Dalm, D., Palm, G.J., Aleksandrov, A., Simonson, T., Hinrichs, W., 2010. Nonantibiotic properties of tetracyclines: Structural basis for inhibition of secretory phospholipase A2. J. Mol. Biol. 398, 83–96. https://doi.org/10.1016/J.JMB.2010.02.049.

Ebadi, A., Soltan Mohammadzadeh, J.S., Khudiev, A., 2009. What is the correct form of BET isotherm for modeling liquid phase adsorption? Adsorption 15, 65–73. https://doi.org/10.1007/s10450-009-9151-3.

EnkeMm, Z.E., Ngangom, B.L., Tamunjoh, S.S.A., Boyom, F.F., 2018. Antibiotic residues in food animals: public health concern. Acta Ecol. Sin. https://doi.org/10.1016/j.chnaes.2018.10.004.

Frisch, M.J., Trucks, G.W., Schlegel, H.B., Scuseria, G.E., Robb, M.A., Cheeseman, J.R., Scalmani, G., Barone, V., Mennucci, B., Petersson, G.A., Nakatsuji, H., Caricato, M., Li, X., Hratchian, H.P., Izmaylov, A.F., Bloino, J., Zheng, G., Sonnenberg, J.L., Hada, M., Ehara, M., Toyota, K., Fukuda, R., Hasegawa, J., Ishida, M., Nakajima, T., Honda, Y., Kitao, O., Nakai, H., Vreven, T., Montgomery, J.A., Peralta, J.E., Ogliaro, F., Bearpark, M., Heyd, J.J., Brothers, E., Kudin, K.N., Staroverov, V.N., Kobayashi, R., Normand, J., Raghavachari, K., Rendell, A., Burant, J.C., Iyengar, S.S., Tomasi, J., Cossi, M., Rega, N., Millam, J.M., Klene, M., Knox, J.E., Cross, J.B., Bakken, V., Adamo, C., Jaramillo, J., Gomperts, R., Stratmann, R.E., Yazyev, O., Austin, A.J., Cammi, R., Pomelli, C., Ochterski, J.W., Martin, R.L., Morokuma, K., Zakrzewski, V.G., Voth, G.A., Salvador, P., Dannenberg, J.J., Dapprich, S., Daniels, A.D., Farkas, Ö., Foresman, J.B., Ortiz, J.V., Cioslowski, J., Fox, D.J., 2009. Gaussian 09 Revision A.2. Wallingford.

Guo, X., Su, G., Li, Z., Chang, J., Zeng, X., Sun, Y., Lu, Y., Lin, L., 2015. Light intensity and N/P nutrient affect the accumulation of lipid and unsaturated fatty acids by Chlorella sp. Bioresour. Technol. 191, 385–390. https://doi.org/10.1016/J.BIORTECH.2015.04.014.

Guo, W.-Q., Zheng, H.-S., Li, S., Du, J.-S., Feng, X.-C., Yin, R.-L., Wu, Q.-L., Ren, N.-Q., Chang, J.-S., 2016. Removal of cephalosporin antibiotics 7-ACA from wastewater during the cultivation of lipid-accumulating microalgae. Bioresour. Technol. 221, 284–290. https://doi.org/10.1016/J.BIORTECH.2016.09.036.

Hanifzadeh, M., Sarrafzadeh, M.-H., Nabati, Z., Tavakoli, O., Feyzizarnagh, H., 2018. Technical, economic and energy assessment of an alternative strategy for mass production of biomass and lipid from microalgae. J. Environ. Chem. Eng. 6, 866–873. https://doi.org/10.1016/J.JECE.2018.01.008.

Hu, X., Jia, L., Cheng, J., Sun, Z., 2019. Magnetic ordered mesoporous carbon materials for adsorption of minocycline from aqueous solution: preparation, characterization and adsorption mechanism. J. Hazard. Mater. 362, 1–8. https://doi.org/10.1016/J.JHAZMAT.2018.09.003.

Kümmerer, K., Henninger, A., 2003. Promoting resistance by the emission of antibiotics from hospitals and households into effluent. Clin. Microbiol. Infect. 9, 1203–1214. https://doi.org/10.1111/j.1469-0691.2003.00739.x.

Li, J., Zhanga, N., Ng, D.H.L., 2015. Synthesis of 3D hierarchical structure of γ-AlO(OH)/MgAl-LDH/C and its performance in organic dyes and antibiotics adsorption. J. Mater. Chem. A 1–10.

Li, L., Abild-Pedersen, F., Greeley, J., Nørskov, J.K., 2015. Surface Tension Effects on the Reactivity of Metal Nanoparticles. J. Phys. Chem. Lett. 6, 3797–3801. https://doi.org/10.1021/acs.jpclett.5b01746.

Liu, M., Zhang, Y., Yang, M., Tian, Z., Ren, L., Zhang, S., 2012. Abundance and distribution of tetracycline resistance genes and mobile elements in an oxytetracycline production wastewater treatment system. Environ. Sci. Technol. 46, 7551–7557. https://doi.org/10.1021/ES301145M.

Lu, L., Li, J., Yu, J., Song, P., Ng, D.H.L., 2016. A hierarchically porous MgFe2O4/γ-Fe2O3 magnetic microspheres for efficient removals of dye and pharmaceutical from water. Chem. Eng. J. 283, 524–534. https://doi.org/10.1016/j.cej.2015.07.081.

Lv, J., Li, Y.M., 2018. Effect of ozonation on minocycline degradation and N-Nitrosodimethylamine formation. J. Environ. Sci. Health A Toxic/Hazard. Subst. Environ. Eng. 53, 617–628. https://doi.org/10.1080/10934529.2018.1429724.

Martin, G.J.O., Hill, D.R.A., Olmstead, I.L.D., Bergamin, A., Shears, M.J., Dias, D.A., Kentish, S.E., Scales, P.J., Botté, C.Y., Callahan, D.L., 2014. Lipid profile remodeling in response to nitrogen deprivation in the microalgae Chlorella sp. (Trebouxiophyceae) and Nannochloropsis sp. (Eustigmatophyceae). PLoS One 9, e103389. https://doi.org/10.1371/journal.pone.0103389.

McKay, G., Otterburn, M.S., Sweeney, A.G., 1980. The removal of colour from effluent using various adsorbents-III. Silica: rate processes. Water Res. 14, 15–20. https://doi.org/10.1016/0043-1354(80)90037-8.

Menegazzo, M.L., Fonseca, G.G., 2019. Biomass recovery and lipid extraction processes for microalgae biofuels production: a review. Renew. Sustain. Energy Rev. https://doi.org/10.1016/j.rser.2019.01.064.

Montes D'Oca, M.G., Viêgas, C.V., Lemões, J.S., Miyasaki, E.K., Morón-Villarreyes, J.A., Primel, E.G., Abreu, P.C., 2011. Production of FAMEs from several microalgal lipidic extracts and direct transesterification of the Chlorella pyrenoidosa. Biomass Bioenergy 35, 1533–1538. https://doi.org/10.1016/J.BIOMBIOE.2010.12.047.

Morgan, D.J., Okeke, I.N., Laxminarayan, R., Perencevich, E.N., Weisenberg, S., 2011. Non-prescription antimicrobial use worldwide: a systematic review. Lancet Infect. Dis. https://doi.org/10.1016/S1473-3099(11)70054-8.

Palm, G.J., Buchholz, I., Werten, S., Girbardt, B., Berndt, L., Delcea, M., Hinrichs, W., 2020. Thermodynamics, cooperativity and stability of the tetracycline repressor (TetR) upon tetracycline binding. Biochim. Biophys. Acta - Proteins Proteomics 1868, 140404. https://doi.org/10.1016/J.BBAPAP.2020.140404.

Pan, L., Cao, Y., Zang, J., Huang, Q., Wang, L., Zhang, Y., Fan, S., Tang, J., Xie, Z., 2019. Preparation of iron-loaded granular activated carbon catalyst and its application in tetracycline antibiotic removal from aqueous solution. Int. J. Environ. Res. Public Health 16, 2270. https://doi.org/10.3390/ijerph16132270.

Parolo, M.E., Avena, M.J., Pettinari, G., Zajonkovsky, I., Valles, J.M., Baschini, M.T., 2010. Antimicrobial properties of tetracycline and minocycline-montmorillonites. Appl. Clay Sci. 49, 194–199. https://doi.org/10.1016/j.clay.2010.05.005.

Pena, A., Paulo, M., Silva, L.J.G., Seifrtová, M., Lino, C.M., Solich, P., 2010. Tetracycline antibiotics in hospital and municipal wastewaters: a pilot study in Portugal. Anal. Bioanal. Chem. 3968 (396), 2929–2936. https://doi.org/10.1007/S00216-010-3581-3, 2010.

R Development Core Team, 2016. R Development Core Team, R: A Language and Environment for Statistical Computing, R Foundation for Statistical Computing. R A Lang. Environ. Stat. Comput.

Saadi, R., Saadi, Z., Fazaeli, R., Fard, N.E., 2015. Monolayer and multilayer adsorption isotherm models for sorption from aqueous media. Korean J. Chem. Eng. 32, 787–799.

Sajjadi, B., Chen, W.Y., Raman, A.A.A., Ibrahim, S., 2018. Microalgae lipid and biomass for biofuel production: a comprehensive review on lipid enhancement strategies and their effects on fatty acid composition. Renew. Sustain. Energy Rev. https://doi.org/10.1016/j.rser.2018.07.050.

Sanganyado, E., Gwenzi, W., 2019. Antibiotic resistance in drinking water systems: occurrence, removal, and human health risks. Sci. Total Environ. 669, 785–797. https://doi.org/10.1016/J.SCITOTENV.2019.03.162.

Scrucca, L., 2013. GA : a package for genetic algorithms in R. J. Stat. Softw. 53, 1–37. https://doi.org/10.18637/jss.v053.i04.

Tran, H.N., You, S.-J., Hosseini-Bandegharaei, A., Chao, H.-P., 2017. Mistakes and inconsistencies regarding adsorption of contaminants from aqueous solutions: a critical review. Water Res. 120, 88–116. https://doi.org/10.1016/J.WATRES.2017.04.014.

Tran, N.H., Reinhard, M., Gin, K.Y.-H., 2018. Occurrence and fate of emerging contaminants in municipal wastewater treatment plants from different geographical regions-a review. Water Res. 133, 182–207. https://doi.org/10.1016/J.WATRES.2017.12.029.

Van Boeckel, T.P., Brower, C., Gilbert, M., Grenfell, B.T., Levin, S.A., Robinson, T.P., Teillant, A., Laxminarayan, R., 2015. Global trends in antimicrobial use in food animals. Proc. Natl. Acad. Sci. U. S. A. 112, 5649–5654. https://doi.org/10.1073/pnas.1503141112.

Wheeler, R., 2004. AlgDesign.

WHO, EMP, IAU, 2019. The 2019 WHO AWaRe Classification of Antibiotics for Evaluation and Monitoring of Use.

Wu, Y., Sun, Y., Zhou, C., Niu, J., 2019. Regeneration of porous electrospun membranes embedding alumina nanoparticles saturated with minocycline by UV radiation. Chemosphere 237, 124495. https://doi.org/10.1016/J.CHEMOSPHERE.2019.124495.

Ye, C., Mu, D., Horowitz, N., Xue, Z., Chen, J., Xue, M., Zhou, Y., Klutts, M., Zhou, W., 2018. Life cycle assessment of industrial scale production of spirulina tablets. Algal Res. 34, 154–163. https://doi.org/10.1016/J.ALGAL.2018.07.013.

Zhang, Z., Liu, H., Wu, L., Lan, H., Qu, J., 2015. Preparation of amino-Fe (III) functionalized mesoporous silica for synergistic adsorption of tetracycline and copper. Chemosphere 138, 625–632.

Zhou, D., Qiao, B., Li, G., Xue, S., Yin, J., 2017. Continuous production of biodiesel from microalgae by extraction coupling with transesterification under supercritical conditions. Bioresour. Technol. 238, 609–615. https://doi.org/10.1016/J.BIORTECH.2017.04.097.